Modelling of Transition and Nucleate Boiling of Liquid Nitrogen Spill on Concrete

Syed Quraishy, Asma Sadia, Tomasz Olewski and Luc Véchot*
Mary Kay O'Connor Process Safety Center (Qatar branch)
Texas A&M University at Qatar, PO Box 23874, Education City, Doha, Qatar
*Corresponding author: luc.vechot@qatar.tamu.edu

Accidental spill of cryogenic liquids like liquefied natural gas (LNG) or liquid nitrogen (LIN) on the ground undergo vigorous boil off due to large temperature difference between the liquid and the ambient condition. Three different boiling regimes can be observed during the spill: film boiling, transition and nucleate boiling.

Heat transfer correlations obtained from the literature were applied to build numerical model of boiling cryogenic liquid spilled on a solid. Different combinations of liquid-solid systems were studied utilizing methane, hydrogen, oxygen and nitrogen on the solid substrates: concrete, soil, aluminium and polystyrene. The boiling curves were generated for a given liquid-solid system and the results were analysed to determine the possibility of occurrence and the duration of each regime during the accidental spill. The analyses show how long each boiling regime can theoretically last for each case. The boiling regime model was compared to simple one-dimensional (1D) "ideal" conduction model, which assumes a semi-infinite solid, heat flux in one direction only and perfect thermal contact at the liquid-solid interface (which leads to constant surface temperature for the solid substrate which is equal to the liquid boiling point). Subsequently, the 1D "ideal" conduction model was modified and extended to account for non-ideal contact at the liquid-solid interface, providing additional resistance for heat transfer to the cryogenic pool.

A set of laboratory and medium scale experiments were performed at the laboratory of Texas A&M University at Qatar and at the Ras Laffan Industrial City (RLIC), Doha, Qatar to provide the validation of these models. The experiments were performed utilizing liquid nitrogen spilled on concrete. To study the effect of surface roughness on vaporization rate of liquid nitrogen, laboratory scale experiments were conducted on rough and smooth concrete surfaces. The vaporization rate was determined directly from the mass loss monitored during the experiments. The film, transition and nucleate boiling regimes were observed during the laboratory scale experiments and nucleate boiling regime was observed in the medium scale experiments. These experiments were used to validate relevant models. Specific heat of the concrete was determined independently by Differential Scanning Calorimetry (DSC) and thermal conductivity was measured by Guarded Hot Plate (GHP) method.

Keywords: Liquid Nitrogen, boiling regimes, vaporization, LNG

Introduction

Environmentally Natural Gas (NG) is the cleanest burning fossil fuel and now a day has become rapidly emerging source of energy. Economically NG produces jobs, benefits community and secures affordable future energy supply. When NG is liquefied, its volume is reduced by about 620 times, thus makes it easier to be transported and stored. Growth of global natural gas trade increased by 1.8% with the progression in pipeline shipments improved by 2.3% in 2013.International LNG trade was recovered by 0.6% in 2013. Imports of LNG increased in South Korea (+10.7%), China (+22.9%) and South and Central American importers (+44.7%) were partly counterbalanced by lesser imports in Spain (-35.6%), the UK (-31.9%) and France (-19.4%). Qatar remained as the largest exporter of LNG (32% of worldwide exports) and accounted for the largest growth increment. Qatar exported 105.6 billion cubic meters (billion m^3) of LNG in 2013 of which 71% to Asia Pacific and 22% to Europe. The total LNG export from Qatar is way beyond than the next largest exporters, Malaysia (33.8 m^3), Australia (30.2 billion m^3), Nigeria (22.4 billion m^3) and Indonesia (22.4 billion m^3) (BP 2014). The world is demanding more energy to power its economies, fuel its industries and improve the living standards of its people. All forms of energy will be needed to encounter the rising demand and it needs to be cost effective, environmentally safe and reliably produced. Many onshore or offshore LNG import terminals are expected to be constructed in the future several years to meet the significant increase in LNG importation from overseas as a result of growing demand (Thorndike 2007). Although LNG industry globally has had a reasonably decent safety record so far compared to other fossil fuels, experienced fatal incidents. The biggest one occurred on 20th of October 1944 in Cleveland, Ohio, where an incorrectly designed tank failed soon after being put into service, causing a LNG release and the formation of flammable vapour cloud. The vapour cloud was ignited and the explosion led to the death of 128 people (Anon 1946; Dweck & Boutillon 2004).

This fast growing industry and accumulating newer technology continuously like Shell's generic Floating LNG (gFLNG), and Shell's another unique patented technology Floating, Liquefaction, Storage and Off-Loading (FLSO*) - adaptable and appropriate for smaller LNG production (Bradley et al. 2005). Constant growth of this industry brings new and novel challenges that require special attention. Therefore, it is vital and tactical to conduct fundamental and applied research in areas related to LNG production, handling and transportation to increase their safety. In 2007, an expert panel formed by US Government Accountability Office has organized a list of research requirements for LNG industry (GAO-07-633T 2007). The Health and Safety Laboratory (HSL), UK while working on a collaborated research with National Fire Protection Association (NFPA) has summarized data for LNG or related field experiments. This database is consists of quality data that can be used for validating mathematical models used for LNG risk assessments. These are good quality data but can only be applicable for neutral atmospheric stability class. According to NFPA 59A guidelines, it is essential to consider LNG release

scenario when weather condition is very stable (stability class F with wind speed 2 ms^{-1}). So having large number of data sets on different weather conditions is a generic requirement.

LNG is usually stored at atmospheric pressure and at its atmospheric pressure boiling temperature of approximately -162^{o}C. If there is any accidental spill or loss of containment on ground surface or water, flammable vapour (predominately methane) will be produced due to the heat transfer to the liquid pool. This generated flammable vapour cloud brings significant fire and explosion hazards. The initially cold vapour resulting from vaporization will be denser than air and forms a dense cloud close to the ground, which is pushed downwind. If an ignition source of sufficient energy is present where a vapour cloud exists at a 4.4%–17% concentration in air, the vapour cloud can ignite and burn. The ability of predicting the vaporization rate of such event is essential for risk assessment of safe separation distances for flammable vapour dispersion and thermal radiation from pool fire. Numerous researches have been performed on the modelling of the vapour cloud dispersion (Cormier et al. 2009; Ivings et al. 2007; Coldrick et al. 2009; Hanna et al. 1993; Hansen et al. 2007; Qi et al. 2010; Woodward & Pitblado 2012). However LNG dispersion analysis is significantly affected by the estimation of source term. The associated source term models have received much less attention despite their critical importance in the prediction of the consequences of a spill (Webber et al. 2010). Indeed, the result of a LNG vapour cloud dispersion simulation is highly sensitive to and dependent on the accuracy of the vapour generation rate calculated from a source term model (Luketa-Hanlin 2006). An accurate source term model is necessary to reduce the uncertainty of the subsequent dispersion model. Substantial efforts are still required in the development and validation of a comprehensive source term model that will be able to describe the physics behind the spreading and vaporization of a LNG pool.

The major reason of having inadequate knowledge on source term models is the deficiency of a comprehensive set of quality experimental data. Without quality data it is quite impossible to draw conclusions on the development and validation of source term models. So, it is evident that experimental data are needed in numerous features related to the source term modelling, including the characteristics of release (flow rate, high momentum jet releases), the rainout, liquid pool spreading and vaporization rate and phenomena (different types of boiling, evaporation) on specific substrate. This paper focuses on vaporisation rate only.

Description of Vaporization Rate Model

When spillage of cryogenic liquid occurs, the rate of vaporization is entirely dependent upon the heat flux provided to the pool. There are several physical mechanisms transporting energy as heat, namely heat conduction, heat convection and heat radiation. These mechanisms can work together in an organized way or by themselves, depending on the real case scenario. In case of spill on the land heat conduction from the ground, heat convection from the ambient air, radiation etc. is considered. These are the main mechanisms of pool vaporization.

The energy balance considering all the heat flow rate is shown below:

$$Accumulated\ Heat = Rate\ of\ heat\ in - Rate\ of\ heat\ out$$
$$\dot{m}\, C_p \frac{dT}{dt} = Q_{cond} + Q_{conv} + Q_{rad} - Q_{evap} \quad (1)$$

Among different modes of heat transfer conductive heat flux plays the most significant role during vaporization of a pool of spilled cryogenic liquid (Woodward & Pitblado 2012) particularly at early stages of the vaporization process. Véchot et al. (2013) investigated the contribution of convective and radiative heat flow to a cryogenic pool and showed that they can play a non-negligible role on the pool vaporization rate at later stages of the vaporization process when the ground has sufficiently cooled down or in the particular case of a spill on an insulated solid substrate. . The work presented in the paper focuses on conductive heat flux from the ground/substrate.

1D Semi-Infinite Heat Conduction Model

Generally, cryogenic liquid vapour formation rate is dominated by the heat transfer from the ground to the liquid pool. All models of cryogenic spill include this phenomenon. However, numerous differences related to the modelling of the heat effects, particularly the boiling of cryogenic upon contact with the ground, and the effect of atmospheric conditions exist. It is commonly applied and accepted that the conductive heat flux is a dominant during the cryogenic pool boiling. Even for conductive heat transfer, the existing models (especially those used in commercial software) tend to overlook the complexity associated with cryogenic pool boiling. A cryogenic liquid spill on an initially hot ground surface will cause this surface temperature to decrease over time. With the assumption of a thin pool, the heat conduction through the ground can be reduced to a one-dimensional (1D) semi-infinite vertical unsteady-state conduction problem described by the Fourier's equation

$$\frac{\partial T}{\partial t} = \alpha \frac{\partial^2 T}{\partial z^2} \quad (2)$$

For spills on land, heat transfer from the ground surface to the cryogenic liquid pool may be modelled using one-dimensional (1-D) heat conduction and assuming the pool is in perfect thermal contact with the ground. This reduces to a 1-D conduction problem in a semi-infinite solid with a Dirichlet type boundary condition (temperature of the ground surface equals to the liquid boiling point) described in Carslaw and Jaeger (1986) and previously used by Briscoe and Shaw (1980).

If perfect thermal contact between the liquid and the ground is assumed, and the ground surface temperature is considered to be constant at the boiling point of the liquid, the solution of equation (2) can be described as:

$$T = T_i - \left(T_i - T_s\right)\mathrm{erfc}\left(\frac{z}{2\sqrt{\alpha t}}\right) \tag{3}$$

where T_i is the initial ground temperature, T_s is the liquid boiling point, z is the vertical distance downwards from the ground surface, α is thermal diffusivity of the ground. The heat flux q from the ground to the pool can be calculated as (Briscoe & Shaw 1980):

$$q = \chi k \left.\frac{\partial T}{\partial z}\right|_{z=0} = \frac{\chi k\left(T_i - T_s\right)}{\sqrt{\pi \alpha t}} \tag{4}$$

where χ is the multiplicative correction factor that accounts for surface roughness, substrate thermodynamic properties and other effects (Briscoe & Shaw 1980)

The above approach is the most commonly used one and requires a good assessment of the thermal properties of the ground. Laboratory-scale experimental data obtained by Reid and Wang (1978) with LNG seem to indicate that a 1-D conduction approach can provide a good representation of the heat transfer into the spreading pool for certain types of concrete substrates.

Boiling Regime Model

Another approach when dealing with heat transfer from the ground would consist on taking into account the different boiling regimes. Cryogens, exhibit vigorous boiling upon release on land or water at ambient temperature resulting from the bubble formation at the liquid-ground interface. Indeed, a large temperature difference between the liquid and the ground would exist at early stages of the spill which will induce vigorous boiling and generate a vapour film at the liquid-ground interface that will act as a barrier to heat transfer from the ground to the pool above. Three boiling regimes are recognized: (1) film boiling (at the initial stage, when the surface is still relatively hot), (2) transition and (3) nucleate boiling (at the later stage, when surface has cooled down). Three-regime boiling has received some attention (Brentari et al. 1965; Berenson 1961; Klimenko 1981; Kalinin et al. 1976; Grigoreyv et al. 1973). Even though there is a lot to be done on the spills on concrete as well as there is a lack of experimental data at the medium and large scale (Webber et al. 2010).

Correlations of different boiling regimes from the literature was used to formulate the boiling curve at different solid-liquid system. Initially the Leidenfrost point was modelled by using film boiling correlation from Kalinin et al. 1976;

$$q_f = 0.18 k_{vf} \Delta T_w \left[\frac{g}{\nu_{vf}\alpha_{vf}}\left(\frac{\rho_l}{\rho_{vf}} - 1\right)\right]^{1/3} \tag{5}$$

$$\Delta T_{\min} = \left(T_c - T_S\right)\left[0.16 + \frac{2.4}{\gamma^{1/4}}\right] \tag{6}$$

Here, $\gamma = \sqrt{\frac{k_w \rho_w Cp_w}{k_l \rho_l Cp_l}}$; is surface-liquid interaction parameter.

The maximum (or critical) heat flux in nucleate pool boiling was determined theoretically from (Kutateladze 1952);

$$q_{Cr} = 0.16 \lambda \rho_v^{1/2} \left[\sigma g (\rho_l - \rho_v)\right]^{1/4} \tag{7}$$

To determine the critical temperature difference ΔT_{Cr}; critical heat flux q_{Cr} was determined from the Kutateladze formula;

$$\Delta T_{Cr} = 0.625\left(q_{Cr}\sigma T_s\right)^{\frac{1}{3}} \frac{\left(\frac{\sqrt{\nu_l}}{k_l} + \frac{10}{\sqrt{\rho_w C_{pw} k_w}}\right)^{\frac{2}{3}}\left(1 + \frac{10}{\gamma}\right)^{\frac{1}{3}}}{\left[1 + 10\left(\frac{\rho_v}{\rho_l - \rho_v}\right)^{\frac{2}{3}}\right]} \tag{8}$$

For nucleate boiling heat transfer an empirical formula by Grigoreyv et al. 1973 is used;

$$q_n = \frac{4.1[1+10\left(\frac{\rho_v}{\rho_l-\rho_v}\right)^{\frac{2}{3}}]^3 \Delta T_w^3}{\sigma T_s (\frac{\sqrt{v_l}}{k_l} + \frac{10}{\sqrt{\rho_w C_{pw} k_w}})^2 \left(1+\frac{10}{\gamma}\right)} \quad (9)$$

Here, $\gamma = \sqrt{\frac{k_w \rho_w Cp_w}{k_l \rho_l Cp_l}}$; is surface-liquid interaction parameter

The heat flux will continue to increase until it reaches a maximum value known as critical heat flux q_{Cr} the corresponding temperature is known as the critical wall superheat ΔT_{Cr}. Kalinin et al. 1976 believed in transition boiling region both nucleate and film boiling coexists. So, they extrapolated the heat flux correlation of the nucleate and film boiling to get a correlation for nucleate boiling. They introduced a new parameter f to describe how much the boiling process is the nucleate boiling regime As shown in the following set correlations:

$$q_t = q_n f + q_f (1-f) \quad (10)$$

$$\Delta T^* = \frac{(\Delta T_w - \Delta T_{Cr})}{(\Delta T_{\min} - \Delta T_{Cr})} \quad (11)$$

$$f = (1-\Delta T^*)^7 \quad (12)$$

Using the above mentioned correlations a boiling curve was generated for different solid-liquid system shown in Figure 1.

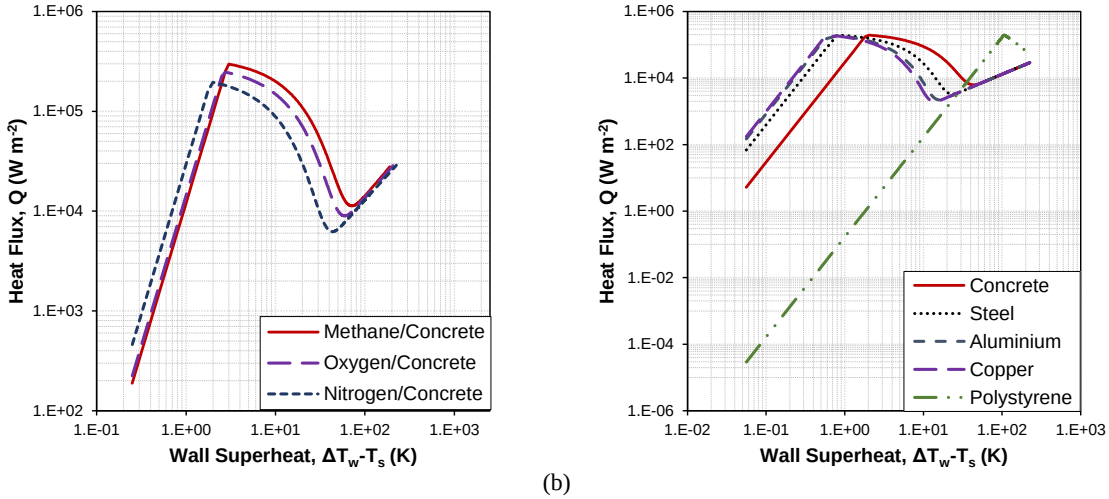

(a) (b)

Figure 1: (a) Boiling Correlation from Kalinin et al. (1976) was applied for different liquids over concrete. (b) Boiling Correlation from Kalinin et al. (1976) was applied for liquid Nitrogen over different substrates

The effect of liquid properties in the pool and the substrate surface is shown in Figure 1. In Figure 1a, the boiling phenomena of different pool liquids (CH_4, O_2, N_2) over the similar substrate concrete is shown. The behaviour of these three liquids at film boiling regime are almost identical and they overlap with each other. The differences are observed in the location of Leidenfrost point and the critical heat flux point. In case of liquid CH_4 vapour film breaks up and Leidenfrost point is reached at lower wall superheat than that of liquid N_2. Liquid O_2 shows intermediate behaviour among these liquids. At CHF point liquid N_2 exhibits lower values in heat flux and wall superheat in comparison with liquid CH_4. The difference is due to the behaviour of vapour film of various liquids formed at the interface and its interaction with the solid substrate at the film boiling regime. At critical point for comparatively low wall superheat the variance of the CHF point for different liquid is due to the surface liquid interaction, active nucleation site density at that specific wall superheat. The boiling curve of liquid N_2 over different (highly conductive metal, non-metal, insulating material) substrates is shown in Figure 1b. To capture the behaviour of cryogenic boiling (liquid nitrogen) on different substrates, a wide range of solid substrates are chosen based on thermal conductivity with concrete having low thermal conductivity and steel having relatively high thermal conductivity.

The insulating material substrate polystyrene does not show any behaviour on the film boiling regime for the temperature range (from liquid N_2 saturation temperature to 50°C) studied. It means that at the initial stage of the spill for given conditions (maximum wall superheat around 246 K), heat flux from polystyrene is not capable of generating enough temperature difference to develop a film at the interface. Other substrates show that all of the three boiling regimes though a variance lies in exhibiting the Leidenfrost point and CHF point. Metals can sustain the temperature difference at the surface for longer time so the film boiling regime is present at comparatively lower wall superheat than concrete (longer duration of film boiling). At CHF point the heat flux value for metal and non-metal is same but this CHF value is achieved at different wall superheat as the latent heat transport from the nucleation sites of different substrates to the liquid is dependent upon the conduction on the thin microlayer below growing bubbles.

For Liquid Nitrogen-Concrete system, boiling correlations from literature (Kalinin et al. 1976) were used to develop a numerical model that takes into account all three different boiling regimes of pool boiling. A Dirichlet type boundary condition to determine the ground temperature is not valid when boiling is considered. This numerical model includes the thermal resistance resulting from the existence of a layer of generated bubbles on the interface between the ground and liquid pool during the boiling process. A Neumann type boundary condition was therefore applied to calculate the ground surface temperature.

The behaviour of the boiling regime model and its comparison with the 1D conduction model is shown in Figure 2 below:

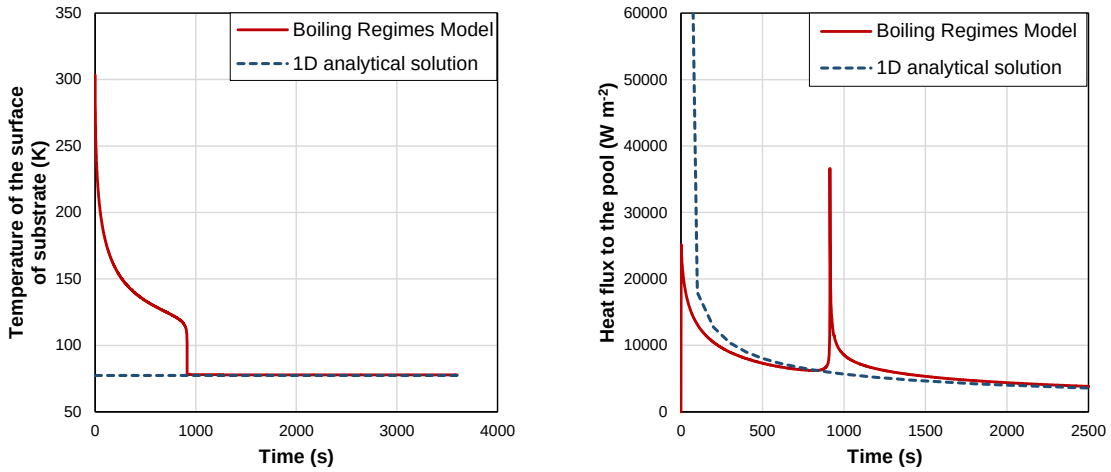

(a) (b)

Figure 2: 1D conduction and boiling regime modelling result comparison for boiling of liquid nitrogen over a concrete; (a) temperature change at substrate surface and (b) heat flux to the pool.

The boiling regime model does not have the limitation of assuming the substrate surface temperature equal to the saturation temperature of the cryogenic pool above it from the beginning of the spill. It is shown in Figure 2a how the substrate surface temperature changes with time. According 1D conduction model the substrate (concrete) surface reaches to the saturation point of the liquid N_2 (77 K or -196 °C) as soon as the liquid touches the ground and it continues to remain at that temperature for the whole time. But for boiling regime model the concrete surface was initially at the ambient temperature (323K or 50 °C) and when the liquid touches the surface it gradually cools down and reaches to the saturation temperature of the liquid after approximately 15 minutes. This delay of reaching to the liquid saturation temperature is due to having a vapour film barrier at the interface. The change in the heat flux with time is shown in Figure 2b. Heat flux for 1D conduction model continues to decrease with time as it assumes perfect thermal contact. But for boiling regime model the heat flux starts to decrease till 15 minutes and then there is a sudden spike which indicates a shift of boiling regime from film to nucleate and then heat flux continues to decrease again in the nucleate boiling regime. The sudden spike (Figure 2b) and the merging of substrate surface temperature with the liquids saturation temperature in (Figure 2a) happens at the same time. These behaviours indicate all three boiling regimes can be captured in the boiling regime model. The boiling regime model predicts the duration of film boiling is 15 minutes then shifts to nucleate boiling .Heat transfer rate during initial stage is lower than 1D conduction model and drops quickly due to the presence of a vapour film acting as barrier.

Experimental setup

To study the contribution of conductive heat transfer mechanism to the vaporization of cryogenic liquid on concrete, well instrumented, laboratory and medium scale experiments were conducted by pouring liquid nitrogen on concrete substrate. It is important to note that the composition of concrete used in both the laboratory and medium scale experiments was the same and is provided in Table 1.

To study the effect of surface roughness on the vaporization of liquid nitrogen, two laboratory scale setups were built with the same dimension and instrumented in a similar way. The substrates used in the two setups consisted of smooth concrete

surface for one setup while rough concrete surface for the other. The smooth surface was obtained by polishing the concrete surface on one side that was to face up.

The surface roughness of each substrate was measured and are provided in Table 2 and is 39.8 and 9.0 µm for rough and smooth concrete, respectively. The standard deviation for smooth concrete was much higher (in relative term) than that of rough one. This effect might be due to the presence of very smooth rocks at the surface of the smooth concrete, which became exposed during the smoothing process. Nearly 30% of the surface of smooth concrete was covered by rocks that are very smooth and have an average roughness as low as 2.9 µm.

Table 1: Composition of concrete in both the laboratory and medium scale experiments

Material	**Batch Weight (kg m^{-3})**	**Fraction (% kg m^{-3})**	**Mass proportion rel. to C**
Dry Portland cement (C)	380	15.6	1
Aggregate 20 mm (A)	676	27.75	3
Aggregate 10 mm (A)	451	18.52	
Washed Sand (S)	766	31.45	2
SP495 (L m^{-3})	7.6	0.31	
Water (L m^{-3})	155	6.36	0.4
Designed density	2435.6	100	
*prepared by Societe d'Entreprise et de Gestion - Qatar W.L.L. Company			

Table 2: Surface roughness of laboratory scale concrete box setup

Concrete surface type	**Average roughness (µm)**	**Standard Deviation (µm)**
Rough concrete surface	39.8	5.1
Smooth concrete surface	9.0	4.7
Very smooth rocks	2.9	1.0

To incorporate the temperature dependent thermal properties of concrete samples they were sent to NETZSCH to obtain the thermal conductivity (using GHP technique) and heat capacity (using DSC technique) as a function of temperature. The result of these analysis is shown in Figure 3. The heat capacity of concrete increase with temperature is consistent with literature (Marshall 1982; Dahmani et al. 2007). However, the increase in thermal conductivity of concrete with temperature is not consistent with literature (Dahmani et al. 2007; Lentz & Monfore 1966). This may be due to the varying concrete properties from literature.

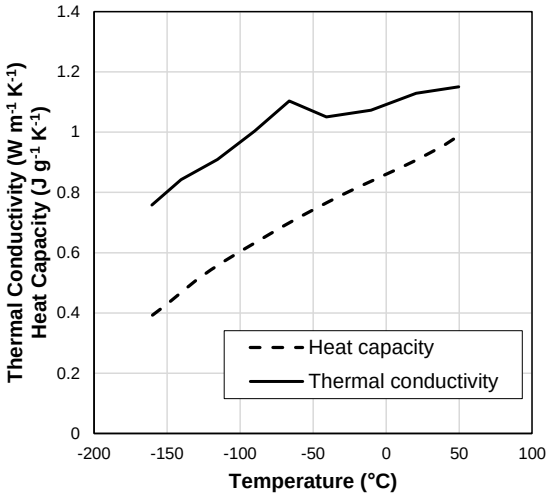

Figure 3: Thermal conductivity and heat capacity obtained as a function of temperature

The 1D conduction model was compared to the experimental results for liquid N_2 Concrete system. Substrate (concrete) thermal properties were evaluated at two temperatures; T_i (temperature at infinite depth of the concrete) and T_b (boiling temperature of the cryogen, LIN). Therefore, there were two values for each property (thermal conductivity, specific heat capacity and thermal diffusivity) and they are provided in Table 3.

Table 3: Thermal properties of concrete at T_i and T_b

Temperature (K)	Thermal conductivity, *k* (W m^{-1} K^{-1})	Specific heat capacity, *Cp* (J kg^{-1} K^{-1})	Thermal Diffusivity, α (m^2 s^{-1})
Ti=297	1.132	915.51	5.30 x 10^{-07}
Tb=77	0.617	259.90	1.02 10^{-06}

Laboratory Scale Experimental Work on Concrete

The laboratory scale experimental setup consisted of two slabs of concrete (30 cm x 30 cm x 5 cm each) as the base with stainless steel walls on all sides. The steel walls were 10 cm high, measured above the top surface of the concrete. The base and the walls of the box were instrumented with a total of eight thermocouples and three heat flux sensors (manufactured by Omega) as shown in Figure 4. The location of the thermocouples and heat flux sensors embedded in the concrete box are provided in Table 4 with origin at the location shown in Figure 4. There were four thermocouples placed in the pool of cryogenic liquid to monitor the temperature of the pool during the experiment. The concrete base box was placed on a Mettler-Toledo balance that had mass measurement precision of 0.1 g. The mass loss of liquid nitrogen, the temperature and heat flux at different locations of the box were recorded at every second of the experiment.

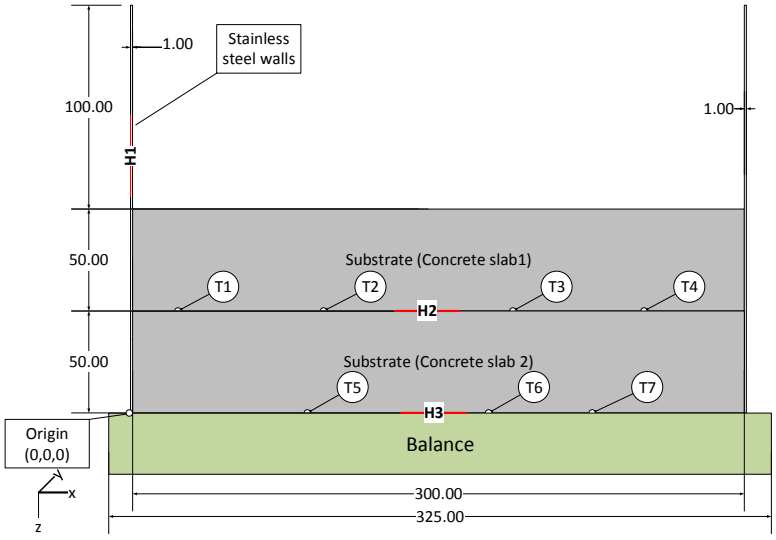

Figure 4: Engineering drawing of the concrete setup in the laboratory (all dimensions are mm)

Table 4: Locations of thermocouples and heat flux sensors in the laboratory scale concrete setup

Thermocouple locations			
Thermocouples	***x* (mm)**	***y* (mm)**	***z* (mm)**
T1	73.0	199.0	50.0
T2	112.0	105.0	50.0
T3	180.0	220.0	50.0
T4	196.0	174.5	50.0
T5	204.5	44.5	50.0
T6	56.0	188.0	0.0
T7	95.0	94.0	0.0
T8	187.5	33.5	0.0

Heat flux sensor locations			
Heat flux sensors	***x* (mm)**	***y* (mm)**	***z* (mm)**
H1	250.0	0.0	80.0
H2	147.0	133.0	50.0
H3	130.0	122.0	0.0

In both the laboratory and medium scale experiments, the balance, the thermocouples and the heat flux sensors were connected to the Data Acquisition system (DAQ) which was provided with an advanced Ethernet-based, 200 kHz rack mountable logger DaqScan/2005 manufactured by IOtech to receive the signals. The DAQ was in turn connected to a computer to read the measurements using DAQView software. This software logs data and saves the recalculated analogue signals in the engineering units of the measured parameters. A LabView program (Virtual instrument – VI) was created to collect the signals from Mettler-Toledo balance, which was not connected to the DAQ.

Medium Scale Experimental Work on Concrete

Medium scale experiment was conducted in a wind tunnel (2 x 2 x 12 m) located at Fire Station 2 at RLIC. The wind tunnel was designed to control the natural convection and limit the solar radiation during the experiment. The prime focus of this experiment was to validate the lab scale experiment and study the vaporization process in a larger scale. The experimental setup consisted of a concrete pad that was instrumented with eleven thermocouples (manufactured by Omega) and two heat flux sensors (manufactured by Hukseflux) embedded inside the pad at four different layers. The location of these sensors are shown in Table 5. These thermocouples allowed monitoring of temperature and heating flux profile inside the concrete that was later used to calculate the heat flux to the pool. The box was built using steel walls at the top of the concrete pad. This box had a capacity of 32 L. The mass loss of liquid nitrogen was measured using a balance. Temperature of the cryogen and the ambient condition data was also monitored by placing thermocouples inside the cryogenic liquid pool and at different location within the wind tunnel respectively. All sensors' output was recorded by a DaqScan/2005.

Cryogenic liquid nitrogen (LIN) was discharged from the cylinder of capacity 180 litres (maximum amount at the site). Cryogenic liquid was spilled through the cryogenic hose by slowly operating a manual valve. During the experiment, the box was placed on a balance (maximum load of 300 kg and resolution of 10 g). The mass of the box was recorded every second and a 30 s averaged LIN vaporisation rate was calculated using mass loss data. LIN was discharged into the containment 5 minutes approximately. Time duration of the spill was determined from opening of manual valve time to the time when the mass on the balance display reached its upper limit. The liquid containment was covered with polystyrene lid to ensure reduced effect of convective and radiative heat transfer to the pool. The measured liquid vaporization rate is directly proportional to the total heat flux to the pool (calculated based on mass loss), which includes the conduction through the ground (concrete base) as well as conduction through the walls and lid. The latter were monitored with heat flux sensors placed on the side and top of walls and lid, respectively. This data was used to remove the heat flux through the wall and lid from the vaporization rate. The schematic of the setup and photos of liquid nitrogen vaporization experiment are shown in Figure 5**.**

Table 5: Locations of thermocouples and heat flux sensors in the medium scale experiment at RLIC

Thermocouple locations			
Thermocouples	***x* (mm)**	***y* (mm)**	***z*(mm)**
TC 106	264.0	120.5	111.0
TC 107	265.0	115.5	226.5
TC 108	132.5	122.5	111.0
TC 109	129.0	119.5	220.0
TC 110	249.0	117.5	28.5
TC 111	320.5	273.5	24.0
TC 112	259.0	119.5	622.0
TC 113	72.5	279.0	33.0
TC 114	312.5	274.0	110.5
TC 115	133.0	122.0	25.0
TC 116	120.0	122.0	621.5
Heat flux sensor locations			
Heat flux sensors	***x* (mm)**	***y* (mm)**	***z*(mm)**
HFS (SN:284) XI103	197.5	168.5	28.5
HFS (SN:285) XI104	193.0	168.5	96.5

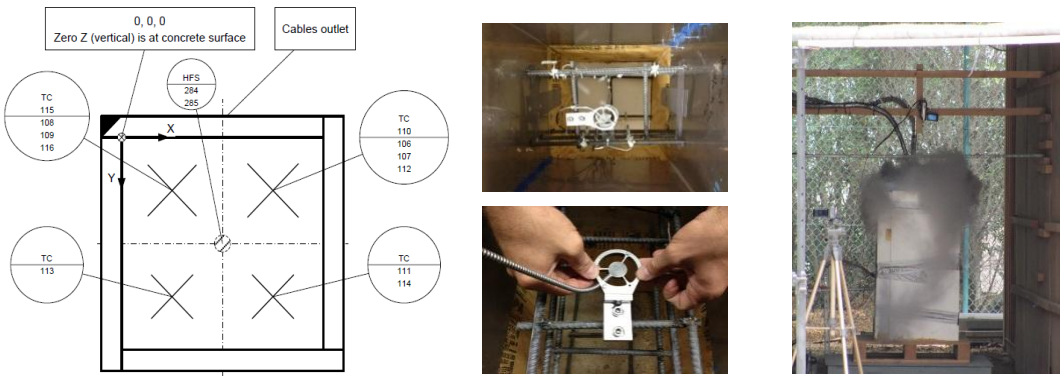

Figure 5: Liquid Nitrogen Spill Experiment over Concrete at RLIC

Methodology and Procedure

Both experiments aimed at studying the contribution of conductive heat transfer mechanism to the vaporization of cryogenic liquid. The effect of surface roughness on vaporization rate was studied in both the laboratory scale and medium scale. To achieve this objective, mass loss of liquid nitrogen and the temperature and heat flux at different locations of the box were recorded at every second. There were 5 runs performed on rough concrete surface and 9 runs on smooth concrete surface for the laboratory scale experiments. Only 3 runs were successful in each experiment (rough and smooth). For the medium scale experiment, six (6) run was performed but for representation only one run was showed in this paper.

The mass loss data was used to calculate the vaporization rate *dm/dt*. For laboratory scale the calculation was done for every second whereas for medium scale the calculation was averaged over 30 s.

The heat flux to the pool q was calculated using (13).

$$q = \frac{\lambda}{A}\frac{dm}{dt} \tag{13}$$

Where L_v is the latent heat of vaporization of liquid nitrogen (199 kJ kg^{-1}), A is the surface area of the substrate that is in contact with the liquid pool and m is the mass of the cryogenic liquid.

Results and analysis

The obtained data were analysed to understand the conductive heat transfer contribution to the vaporization rate of LIN on rough and smooth surface of concrete to study the effect of surface roughness. The effect of scaling on the vaporization rate of LIN was also studied. The results were compared to 1D conduction model by incorporating the thermal properties of the substrate as a function of temperature.

For the laboratory scale experiments, the vaporization rate versus time curve of three successful runs namely, runs 3, 4 and 5 for rough concrete surface and runs 7, 8 and 9 for smooth surface concrete, are shown in Figure 6a and b, respectively. All test runs show similar trend and no significant difference is observed within the test runs. Therefore, it can be concluded that the laboratory scale experimental runs were reproducible.

There were two boiling regimes (transition and nucleate) observed in the spill of LIN on rough concrete (Figure 6a) and three boiling regimes (film, transition and nucleate) observed on smooth concrete (Figure 6b).

The data analysis was carried out after 5 s from the start of the experiment because the spill of liquid nitrogen took 2-3 seconds and the cryogenic pool became stable after 5 seconds of the start of spill. As shown in Figure 6a, the first boiling regime that appears is the transition regime which lasts until the 25th second from the start of spill. The maximum vaporization rate of 31.33 g s^{-1} (average of all runs) is reached at 25 s, which is the time at which there is a shift of boiling regime from transition to nucleate. The heat flux at this time is maximum and is called the critical heat flux (CHF). The average value of CHF for all the runs is 69.28 kW m^{-2}. After the CHF point, the vaporization rate and consequently, the heat flux from the ground decreases due to cooling of the substrate by the cryogenic liquid. Although film boiling regime was not observed on rough concrete, it is important to note that the presence of this regime cannot be completely disregarded. If this regime existed, then it was in the first 5 seconds of the cryogenic liquid spill on the surface. Since film boiling regime was not observed, the minimum boiling heat flux called the Leidenfrost point was not determined for spill experiments on rough concrete.

As shown in Figure 6b, the first boiling regime that appears is the film boiling regime that lasts for 20 s from the start of spill. The minimum vaporization rate at the end of film boiling regime is 14.63 g s^{-1} (average of all runs) which corresponds to the average minimum heat flux or Leidenfrost point of 32.34 kW m^{-2}. The transition regime begins at 20 s which lasts

until 90 s from the start of spill. The maximum vaporization rate of 24.02 g s^{-1} (average of all runs) is reached at 90 s, which is the time at which there is a shift of boiling regime from transition to nucleate. The CHF is 53.10 kW m^{-2}.

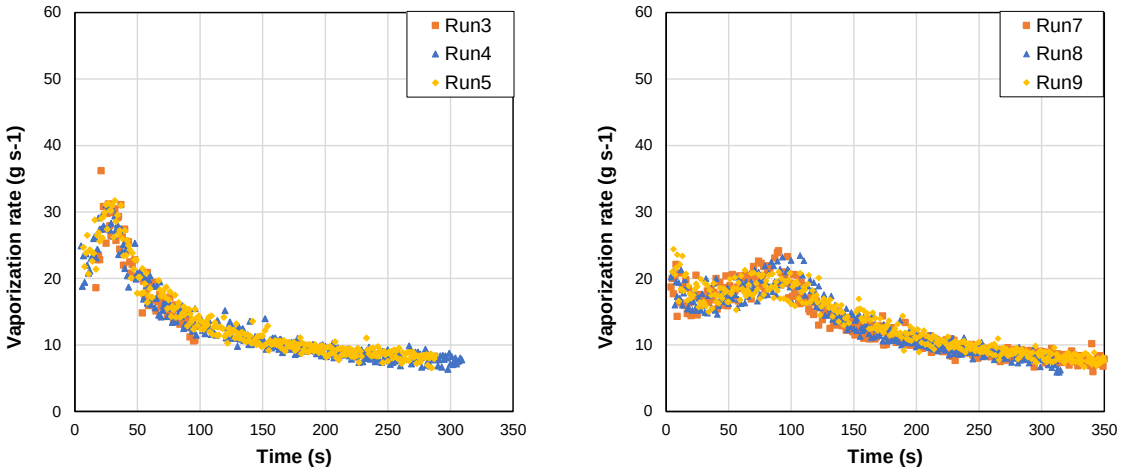

(a) (b)

Figure 6: Repeatability of the laboratory scale experiments on rough (a) and smooth (b) concrete surface

A log plot of heat flux to the pool as a function of time is shown in Figure 7. Both rough and smooth concrete surface laboratory experiments were plotted on this graph alongside medium scale RLIC experimental data. The 1D model was plotted by evaluating concrete thermal properties at two temperatures, initial temperature of the concrete during the experiment (T_i) and boiling temperature of LIN (T_b).

In the case of laboratory scale experiments, the nucleate boiling heat flux is smaller for higher surface roughness (Figure 7). The transition boiling heat flux is higher for boiling of LIN on rough concrete. The CHF increases with increase in surface roughness. The onset of nucleate boiling regime is delayed on smooth concrete surface. Since the film boiling was not observed for spill on rough concrete, it is clear that the Leidenfrost point is dependent on surface roughness. Therefore, the film boiling regime is also dependent on surface roughness.

The experiments conducted in both the laboratory and medium scales were on the same type and composition of concrete. It is important to note that the medium scale concrete surface was rough and no smoothing techniques was applied to the surface. Therefore, the heat flux to the pool vs. time curve for laboratory scale rough concrete and medium scale concrete were expected to overlap. Instead, the medium scale experimental heat flux to the pool was found to be lower than laboratory scale experimental heat flux (Figure 7). The lower heat flux in the medium scale experiment can be attributed to the surface roughness being higher on medium scale concrete.

Figure 7 shows that the 1D conduction model evaluated with concrete thermal properties at T_i over predicts the laboratory experimental results in the beginning for few seconds and then under predicts the data. The model is able to predict the medium scale experimental results. However, the 1D conduction model evaluated with properties of concrete at T_b under predicts experimental data obtained at both scales. It is important to note that, in all these cases, the value of the correction factor, χ, has been taken as 1.

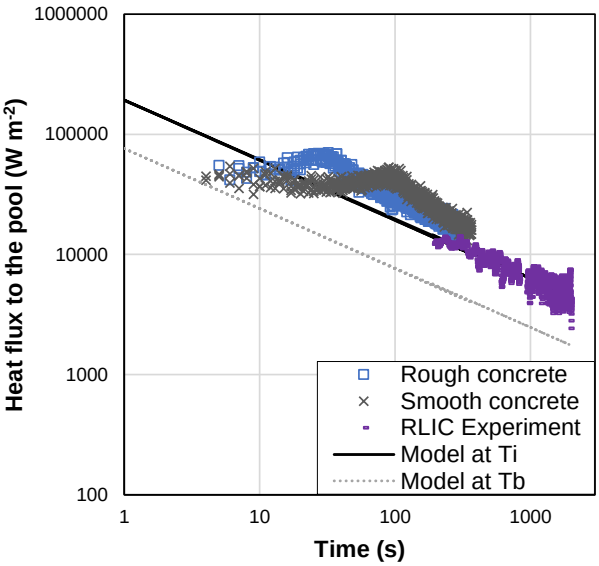

Figure 7: Comparison of rough and smooth concrete surface laboratory experiments with medium scale experiments. 1D model (dashed line), experimental data (marker points)

Conclusions

This study investigated the contribution of conductive heat transfer mechanism to the vaporization of liquid nitrogen on concrete. The effect of surface roughness was also studied in the laboratory scale, on rough and smooth concrete surface. The obtained laboratory experimental results were compared with medium scale RLIC results and the 1D conduction model.

The laboratory experimental results showed good reproducibility. They show the presence of transition and nucleate boiling regimes on rough concrete and all three boiling regimes on smooth concrete. The CHF was found to increase with the surface roughness. The nucleate boiling heat flux was higher for smooth concrete and the transition boiling heat flux was higher for rough concrete. The film boiling was found to be dependent on surface roughness. Since the medium scale experimental results show nucleate boiling regime with lower heat flux than the rough concrete experimental results, the medium scale concrete has a higher surface roughness than the laboratory scale concrete. Therefore, if the surface roughness is constant, there is a high possibility of overlap between the laboratory scale and medium scale data.

The 1D conduction model, which is currently used in commercial software, underpredicts the experimental results when concrete thermal properties are evaluated at T_i and T_b (without any consideration of χ parameter). Therefore, the model requires improvement for good estimation of the experimental data. One way to improve could be to quantify χ parameter.

Acknowledgement

The authors would like to acknowledge the long term, not only financial, support provided by Qatar National Research Fund (QNRF) for the LNG safety research being conducted at Texas A&M University at Qatar (TAMU at Qatar). They also acknowledge the support of Qatar Petroleum in the form of the facilities used for experiments at RLIC and the provision of staff to work with the TAMU at Qatar's LNG research team.

Author contributions

T.O. conceived the idea and designed the experiments. S.Q. and T.O. prepared and conducted a medium scale experiment. A.S., T.O. and L.V. prepared and conducted a laboratory experiment. S.Q. developed the theoretical description and performed the numerical modelling. A.S., S.Q. and T.O. co-wrote the paper. L.V. supervised the project. All authors contributed to the discussion and data analysis.

Nomenclature

A Surface area of the substrate that is in contact with the liquid pool (m^2)

T Temperature (K)

T_i Initial temperature of the ground (K)

T_s	Cryogenic boiling temperature (K)
T_c	Critical temperature (K)
t	Time (s)
F	Extrapolation parameter for transition boiling
g	gravitational acceleration
z	Vertical distance downward from the surface of the ground (m)
m	Mass of cryogenic liquid (kg)
Q_{Cond}	Conductive heat flux to the pool
Q_{Conv}	Convective heat flux to the pool
Q_{rad}	Radiative heat flux to the pool
Q_{eva}	Evaporative heat flux out of the pool
q	Heat flux from the ground to the pool (W m^{-2})
q_f	Heat flux at the film boiling regime
q_C	Critical heat flux
q_n	Heat flux at the nucleate boiling regime
ΔT_{Cr}	Critical wall superheat (K)
ΔT_{min}	Minimum wall superheat (K)
ΔT^*	Dimensionless wall superheat

Greek Symbols

α	Thermal diffusivity of the ground (m^2 s^{-1})
σ	Surface Tension (N m^{-1})
γ	Surface-liquid interaction parameter (dimensionless)
ρ	Density (kg m^{-3})
λ	Latent heat of vaporization (J kg^{-1})
χ	Multiplicative correction factor
ν	Kinematic viscosity (m^2 s^{-1})

Subscripts

w	Wall
v	Vapour phase
l	Liquid phase
vf	Vapour film
i	Initial
s	Saturated Condition
c	Critical Condition
f	Film boiling
t	Transition boiling
n	Nucleate boiling

References

Anon, 1946. *U.S. Bureau of Mines. Report on the Investigation of the Fire at the Liquefaction, Storage, and Regasification Plant of East Ohio Gas Co., Cleveland, Ohio, October 20, 1944.*,

Berenson, P.J., 1961. Film-boiling heat transfer from a horizontal surface. *Journal of Heat Transfer*, pp.351–356. Available at: http://www.osti.gov/energycitations/product.biblio.jsp?osti_id=4006957 [Accessed September 27, 2012].

BP, 2014. BP Statistical Review of World Energy June 2014. , (June).

Bradley, A. et al., 2005. Innovation in the LNG Industry : Shell's Approach.

Brentari et al., 1965. Nucleate and Film Pool Boiling Design Correlation. *Advanced Cryogenic Engineering*.

Briscoe, F. & Shaw, P., 1980. Spread and Evaporation of Liquid. *Progress in Energy and Combustion Science*, 6(2), pp.127–140.

Carslaw, H.S. & Jaeger, J.C., 1986. *Conduction of Heat in Solids* 2nd ed., Oxford University Press, USA.

Coldrick, S., Lea, C.J. & Ivings, M.J., 2009. *Validation Database for Evaluating Vapor Dispersion Models for Safety Analysis of LNG Facilities*, Available at: http://www.nfpa.org/foundation.

Cormier, B.R. et al., 2009. Application of computational fluid dynamics for LNG vapor dispersion modeling: A study of key parameters. *Journal of Loss Prevention in the Process Industries*, 22, pp.332–352.

Dahmani, L., Khenane, A. & Kaci, S., 2007. Behavior of the reinforced concrete at cryogenic temperatures. *Cryogenics*, 47(9-10), pp.517–525. Available at: http://linkinghub.elsevier.com/retrieve/pii/S0011227507000999 [Accessed June 11, 2012].

Dweck, J. & Boutillon, S., 2004. Deadly LNG incident holds key lessons for developers, regulators. *Pipeline and Gas Journal*, 231, pp.39–42.

GAO-07-633T, 2007. *Maritime Security: Public Safety Consequences of a Liquefied Natural Gas Spill Need Clarification*, Washington, DC 20548. Available at: www.gao.gov/cgi-bin/getrpt?GAO-07-633T [Accessed November 14, 2011].

Grigoreyv et al., 1973. Boiling of Cryogenic Fluids. *Journal of Thermal Engineering*, 9(57), p.p. 289.

Hanna, S., Chang, J. & Strimaitis, D., 1993. Hazardous gas model evaluation with field observations. *Atmospheric Environment. Part A. …*, 27(15). Available at: http://www.sciencedirect.com/science/article/pii/096016869390397H [Accessed September 10, 2012].

Hansen, O.R., Melheim, J.A. & Storvik, I.E., 2007. CFD-modeling of LNG dispersion experiments. *AIChE Spring National Meeting, …*, (April). Available at: http://www.gexconus.com/doc/olav/LPS_Houston_Hansen_2007.pdf [Accessed September 10, 2012].

Ivings, M.J. et al., 2007. *Evaluating Vapor Dispersion Models for Safety Analysis of LNG Facilities*, THE FIRE PROTECTION RESEARCH FOUNDATION.

Kalinin, E.K. et al., 1976. Heat transfer in transition boiling of cryogenic liquids. *Advances in Cryogenic Engineering*, 21, pp.273–277.

Klimenko, V.V., 1981. Film boiling on a horizontal plate - new correlation. *International Journal of Heat and Mass Transfer*, 24(1), pp.69–79. Available at: http://linkinghub.elsevier.com/retrieve/pii/0017931081900946.

Kutateladze, S., 1952. Heat Tarnsfer in Condensation and Boiling.

Lentz, A.E. & Monfore, G.., 1966. Thermal Conductivities of Portland Cement Paste, Aggregate, and ConcreteDown to Very Low Temperatures. *Journal of the PCA Research and Development Laboratories*, 8(3), pp.27–33.

Luketa-Hanlin, A., 2006. A review of large-scale LNG spills: Experiments and modeling. *Journal of Hazardous Materials*, 132(2-3), pp.119–140.

Marshall, A.L., 1982. Cryogenic concrete. *Cryogenics*, (November), pp.555–565.

Qi, R. et al., 2010. Numerical simulations of LNG vapor dispersion in Brayton Fire Training Field tests with ANSYS CFX. *Journal of Hazardous Materials*, 183(1-3), pp.51–61. Available at: http://dx.doi.org/10.1016/j.jhazmat.2010.06.090.

Reid, R.C. & Wang, R., 1978. The boiling rates of LNG on typical dike floor materials. *Cryogenics*, 18(7), pp.401–404.

Thorndike, V.L., 2007. *LNG: A Level-Headed Look at the Liquefied Natural Gas Controversy*, Down East Books.

Véchot, L. et al., 2013. Laboratory scale analysis of the influence of different heat transfer mechanisms on liquid nitrogen vaporization rate. *Journal of Loss Prevention in the Process Industries*, 26(3), pp.398–409. Available at: http://linkinghub.elsevier.com/retrieve/pii/S0950423012001155.

Webber, D.M. et al., 2010. *LNG source term models for hazard analysis: A review of the state-of-the-art and an approach to model assessment*, Buxton, Derbyshire, UK. Available at: http://www.hse.gov.uk/research/rrpdf/rr789.pdf.

Woodward, J.L. & Pitblado, R., 2012. *LNG Risk Based Safety - Modeling and Consequence Analysis*, Hoboken, NJ, USA; Published simultaneously in Canada: AIChE, John Wiley & Sons, Inc.